

Performance Analysis of Multiport Antennas in Vehicle-to-Vehicle Communication Channels

Abed Pour Sohrab ^{1*}, Yingke Huang ², and Petros Karadimas ³

¹Avery Dennison UK Ltd. Chelmsford, UK

²James Watt School of Engineering, University of Glasgow, Scotland, UK

³School of Computing, Engineering and the Built Environment, Edinburgh Napier University, Scotland, UK

poursohrab@gmail.com, p.karadimas@napier.ac.uk,
Y.Huang.2@research.gla.ac.uk

Abstract. A holistic performance analysis and classification of multiport antennas (MPAs) is conducted in this paper. We focus on 5.9 GHz vehicle-to-vehicle (V2V) communications suited to the emerging technology of intelligent transportation systems (ITS). Three-dimensional (3-D) uniform/isotropic, directional, and omnidirectional propagation scenarios are considered to account for any wireless environment. The presented analysis can be adapted to any MPA with an arbitrary number of ports, operating in any frequency band, or used in other emerging technologies such as in 5G and beyond 5G communications. On top of the classical key performance metrics (KPMs) in communication theory, i.e., the diversity antenna gain (DAG) and channel capacity (CC), we employ for the first time the energy efficiency (EE) as one more KPM capable to characterize performance and classify MPAs, particularly when DAG and CC fail to do so. Computation of the aforementioned KPMs departs from a covariance matrix formulation incorporating all intrinsic features that affect MPA performance, namely, MPA radiation characteristics, MPA termination conditions, and wireless propagation channel attributes. Accordingly, we derive the ideal form of the covariance matrix under the standardized and widely adopted 3-D uniform/isotropic wireless propagation scenario. A good MPA design should be one with a covariance matrix as close as possible to this ideal one. The adopted performance analysis methodology can thus inform the design of optimum MPAs and accordingly, we designed a proof-of-concept box-shaped MPA which shows outstanding performance across all propagation scenarios. It would be wise to conduct similar performance analyses as in this paper before releasing an MPA design.

Keywords: Channel capacity· Covariance matrix· Diversity antenna gain· Energy efficiency· Multiport antenna systems.

1 Introduction

Advancement of intelligent transportation systems (ITS) and development of fifth generation (5G) technology will establish a network of connected devices, vehicles, and individuals [1]-[3]. Use of multiport antennas (MPAs) in wireless devices can accommodate parallel data streams [4]. An MPA should be carefully designed to achieve optimum performance in every wireless propagation environment. Thus, performance evaluation of MPAs in realistic wireless propagation conditions is of paramount importance in order to identify which designs are the optimum and direct future research in devising even better MPAs. Performance varies in different propagation environments also depending on the MPA's termination circuit and radiation characteristics. However, there is a lack of comprehensive and comparative studies on the performance evaluation of state-of-the-art MPAs operating in different wireless propagation environments. The latter is treated in this paper where we study the performance of the end-to-end MPA wireless system comprised of the following interconnected components, namely, a) termination circuit, b) MPA, c) wireless propagation channel.

The three-dimensional (3-D) uniform/isotropic propagation scenario has been widely employed to characterize capacity and diversity performance of MPAs [5], [6]. However, 3-D uniform propagation is not always the case and directional scenarios such as Gaussian, Laplacian, and von Mises can model realistic wireless propagation conditions [7]-[10]. In this paper, we comprehensively and comparatively study the performance of MPAs in 5.9 GHz vehicle-to-vehicle (V2V) communication channels for all classes of 3-D propagation scenarios, namely, 3-D uniform, 3-D

directional, 3-D omnidirectional. In particular, we consider the following scenarios: a) 3-D uniform or 3-D isotropic having uniform power angle spectrum (PAS) in both azimuth and elevation, b) 3-D directional having Gaussian PAS in both azimuth and elevation, c) 3-D omnidirectional having uniform PAS in azimuth and Gaussian PAS in elevation. The benefit of conducting performance analyses in a complete set of wireless propagation scenarios was demonstrated in our recently published paper [11]. In the open literature, even in the most recently published works, MPA performance evaluation is usually conducted under a) and/or c) settings, thus, findings are constrained to the adopted wireless propagation scenario, e.g., [12]. We focus on V2V communications because they are regarded as a key enabler of future ITS with autonomous driving capabilities [13]. The presented analysis can be readily adapted to any other setting and emerging technology, such as MPAs for 5G and beyond 5G wireless networks.

Various key performance metrics (KPMs) such as the envelope correlation coefficient (ECC), total active reflection coefficient (TARC), and mean effective gain (MEG) are usually employed to evaluate the performance of MPAs [14]. We adopt the diversity antenna gain (DAG) and channel capacity (CC) as the most universal KPMs in communication theory to characterize performance [6], [15]. Considering the dual-branch maximal ratio combining (MRC) diversity as an example, the maximum theoretical DAG in the standardized Rayleigh, dual-polarized, 3-D uniform propagation scenario is equal to 8.71 dB at 1% outage probability (OP). An optimum dual-port antenna is meant to perform as close as possible to this maximum level. We clearly demonstrate that CC performance follows DAG performance, a result that can be implicitly deduced from the analysis in [16], [17]. Thus, we focus on CC performance for the remaining propagation scenarios. As Rayleigh fading just accounts for purely diffusive propagation, Rician fading that physically incorporates a strong line-of-sight (LOS) component will be further considered in the 3-D directional and omnidirectional scenarios to further generalize our analysis.

We introduce the energy efficiency (EE) as an additional KPM capable of characterizing and comparing different MPAs, particularly when DAG and CC fail to do so. The EE is defined as the ratio of CC to total power consumption [18]. In turn, the total power consumption consists of the transmitted power and power consumptions incurred by the circuitry. Various power consumption models have been presented in previous works [18]–[23]. A simplified model was presented in [19], [20] depending on transmitted power and considering constant circuit power. Expanding circuit power modeling, the impact of signal processing power consumption was incorporated in [18], [21]–[23]. The power models presented in [19]–[22] are limited to static circuit power, whereas the ones in [18], [23] rely on dynamic circuit power models varying with CC. In this paper, we consider both static and dynamic classification of circuit power consumption models. For comparison, the models of [19] and [18] are selected to account for static and dynamic circuit power consumption, respectively. Both models are applied for the first time in the similar problem of performance evaluation of MPAs and it is demonstrated the benefit of energy efficiency to characterize and compare different MPAs, particularly when DAG and CC fail to distinguish which MPA performs better. We rigorously demonstrate EE performance with respect to the transmitted power and not just with respect to CC as was practiced before [19]. Starting with 3-D uniform/isotropic propagation, the dynamic model [18] predicts a reasonable monotonic decrease of EE with respect to CC, whereas the simplified static model [19] results in a global maximum before the monotonic decrease. Thus, the dynamic circuit power consumption model can be more reasonable in estimating realistic power consumptions compared with the static one. Therefore, we will adopt this model to determine the EE for the remaining 3-D propagation scenarios. It is shown that EE conforms to CC and DAG, i.e., MPAs with better CC and DAG performance are expected to have better EE. More importantly, when MPAs cannot be sufficiently discriminated by CC and DAG, this can be done by EE. EE is thus proven to be a complementary to DAG and CC KPM that can sufficiently characterize MPA performance.

The foundation of the three aforementioned KPMs is the covariance matrix, which determines the correlation between the port voltages. In MPA analysis and design it is of paramount importance to accurately derive the covariance matrix by adopting standardized antenna terminology [24]. The elements of the covariance matrix have been traditionally calculated using the MEG and ECC [25], [26]. This method cannot rigorously incorporate MPA radiation attributes and impedance matching. However, we demonstrate that MEG and ECC can be leveraged to determine the ideal form of the covariance matrix in the dual-polarized, 3-D uniform propagation scenario and an MPA with uncorrelated port voltages would have such an ideal covariance matrix form. The 3-D uniform propagation scenario has its own merit as it is a standardized and widely adopted one enabling performance evaluation with respect to MPAs' exclusive radiation pattern attributes [27]. The ideal form of the covariance matrix is extremely important as it can inform MPA designers of how close to optimum their design is. The covariance matrix of realistic MPAs is not expected to be exactly equal to the ideal due to impedance mismatches and imperfect radiation efficiencies. But a good MPA design is expected to have a covariance matrix close to the ideal one. In this paper, we employ the purely electromagnetic method proposed in [24] to accurately determine the covariance matrix. It does not rely on MEG and ECC, but rigorously incorporates MPA radiation attributes and impedance matching via standardized IEEE antenna terminology. It can thus explicitly account for the impact of the different subsystems comprising the whole MPA system, that is, a) termination circuit, b) MPA, c) wireless propagation channel.

The remainder of this paper is organized as follows: MPA designs are reviewed in Section 2. The system model and propagation scenarios for V2V communications are presented in Section 3. The DAG, CC, and EE KPMs are presented in Section 4. Performance analysis of selected MPAs is conducted in Section 5. Section 6 draws the conclusion.

2 Relevant MPA Designs

In the following we briefly review previous MPA systems and their performance evaluation methodologies. The isolation between the two antennas of the MPA was improved by using modified ground plane in [28]-[33]. The ground plane creates pattern diversity by directing the main lobe of the two antennas to different directions. The main metrics employed in [28]-[33] were the ECC and DAG. In addition to them, TARC was evaluated in [28], MEG and TARC in [29], [30], and CC in [32]. Composite right-left-handed (CRLH) elements were employed in some works to make compact MPAs [34]. The performance of such design was evaluated by using the ECC, DAG, and CC loss. A wideband neutralization line was used to reduce the mutual coupling between the closely located ports in [35], but without conducting performance evaluation. Size reduction was achieved in [36] by proposing a miniaturized Yagi-based MPA and its outstanding performance was verified in [37] by using the diversity measure. Polarization diversity is another direction for compact MPA design. An orthogonal dual element design was proposed in [38] with the main lobe of the antennas being perpendicular to each other. ECC and MEG were evaluated for this design. Size compression can be also achieved by using a shared radiator structure for orthogonal transmission modes as suggested in [39], [40]. The ECC for both designs was evaluated together with the DAG for the design in [40]. The aforementioned modified ground plane, polarization diversity, and shared radiator techniques have also been employed in designing 4-port [41]-[47] and 8-port MPAs [48]-[50]. The classical performance metrics of ECC and MEG were mainly employed for these MPAs. Evaluation of all the reviewed works took place in 3-D uniform Rayleigh fading scenarios. However, neither directional propagation, nor Rician fading were considered, as is the case in realistic wireless channels. Most of the previous works designed compact MPAs with a focus on reducing the correlation between the ports.

Many of the reviewed designs from the literature are similar in terms of size and type of antenna elements. Consequently, they exhibit similar gain and radiation pattern and will perform evenly in different propagation scenarios. The designs were thus categorized in terms of structure, radiation pattern, gain, size, and polarization along the way of our analysis. Four designs which show better performance at 5.9 GHz for vehicular communications are selected to be evaluated in this paper. The first design is the broadband shared radiator antenna introduced in [39]. The idea of this design is to use the same radiator patch for both antenna ports having orthogonal polarization. This would decrease the overall dimensions of the MPA being already of smaller size from the one in [40]. The broadband working frequency of the MPA is in the range of 2.4-12.75 GHz with a gain of 4.5 dBi at 5.9 GHz. The second design is an ultra-wide-band (UWB) monopole antenna for automotive communications proposed in [31]. Monopole antenna elements are promising options in designing MPAs. The frequency response and radiation pattern of such antennas can be easily modified by manipulating the radiator and ground structure. The radiator of the UWB monopole antenna is comprised of a combination of half circular ring and half square ring. This special design along with the modified ground plane offers an UWB frequency response which covers 3.1-10 GHz with gain of 3.1 dBi at 5.9 GHz. Impedance matching at certain frequencies was improved in [51] via optimization techniques. Different arrangements of two antennas to form an MPA were suggested in [31]. The arrangement that is used in this paper is shown in [31, Fig. 7 (b)]. The third design is a dual-port wideband Yagi-based antenna presented in [36]. The antenna can cover the 5.9 GHz band having 4.183-6.584 GHz working frequency range. This design was selected because it has two significant characteristics. First, its size is larger than usual dual-port antennas. Second, the radiation patterns of the two elements are almost aimed in the same direction. Hence, it is expected to perform differently compared with the other designs having pattern or polarization diversity. According to the relatively large dimensions of this design, and with the help of a director element, the directivity and gain can reach up to 6.6 dB and 6 dBi respectively. Its outstanding diversity performance in the 3-D uniform propagation scenario was evidenced in [37].

The fourth design is a box-shaped slot antenna which was originally demonstrated in our conference paper [52]. This MPA was designed as proof-of-concept to perform outstandingly in all wireless propagation scenarios. For that purpose, certain design features have been tuned including the length and position of the microstrip feed and the dimensions of the slot. The good impedance matching and isolation of the ports along with the high radiation efficiency of 92% guarantees an optimum performance close to the maximum theoretical limit in the standardized Rayleigh dual-polarized, 3-D uniform propagation scenario. In addition, the box-shaped structure is carefully designed to increase the gain of the antenna up to 6.5 dBi which ensures a promising performance in the purely directional scenario having Gaussian PAS in both the azimuth and elevation. Four slots are arranged on each side of the box to have the radiation pattern evenly distributed around the structure. This guarantees outstanding performance in the omnidirectional scenario having

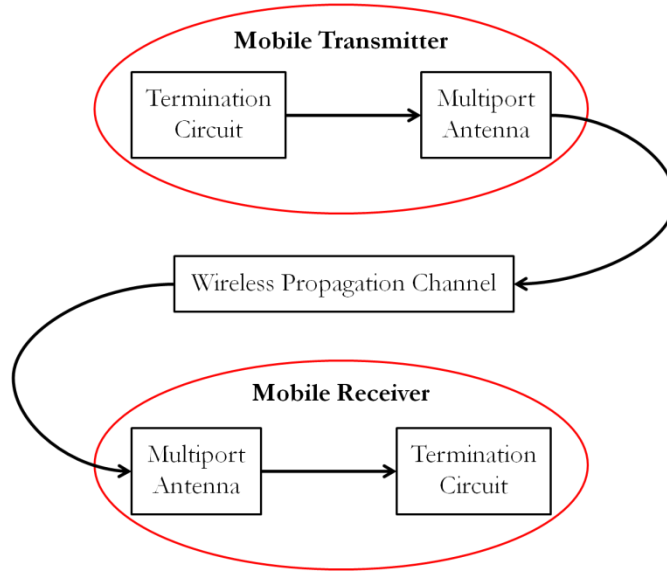


Fig. 1. Block diagram of the end-to-end wireless communication system.

uniform PAS in azimuth and Gaussian PAS in elevation. Such a proof-of-concept MPA can instigate researchers and readers to conduct further research and devise optimum MPAs informed by holistic performance analyses.

DAG, CC, and EE of the four MPAs discussed above [39], [31], [36], [52] are determined and compared with each other. Such performance evaluations and comparisons can underpin optimum MPA design or selection of the optimum one according to the propagation channel attributes. The main contributions of this paper are summarized below:

- Performance evaluation of end-to-end MPA systems in a complete set of wireless propagation scenarios (3-D uniform, 3-D directional, 3-D omnidirectional under Rayleigh and Rician fading) is conducted for the first time. We consider dual-port antennas for 5.9 GHz V2V communications as case study, but the analysis can be readily adapted to designs with more ports and in different frequency bands and communication channels.
- EE is introduced as an additional KPM, complementary to DAG and CC, capable of characterizing performance and comparing different MPA systems particularly when DAG and CC fail to do so.
- The ideal covariance matrix form in the standardized and widely adopted dual-polarized, 3-D uniform propagation scenario is determined to inform optimum MPA design and calibration.
- A proof-of-concept box-shaped MPA (see [52]) has been carefully designed that can perform outstandingly in all wireless propagation scenarios.
- Outstanding performance of the Yagi-based MPA [36] is revealed through comparisons in all wireless propagation scenarios. Thus, findings of [37] arisen from just 3-D uniform propagation in Rayleigh fading are complemented.

3 System Model and Propagation Scenarios

In the following, we present the wireless communication system model and the selected propagation scenarios.

3.1 System Model

The block diagram of the end-to-end wireless communication system adopted in this paper is shown in Fig. 1. As MPA performance analysis has its foundation on the covariance matrix formulation presented in [24], which considers the MPA radiation characteristics, the MPA termination conditions, and the wireless propagation channel attributes as independent factors affecting performance, the mobile transmitter (Tx) and receiver (Rx) each include a termination circuit-MPA sub-system. These sub-systems are physically connected via the wireless propagation channel. The wireless propagation channel constitutes a shared component bonding the two sub-systems, resulting in a termination circuit-MPA-propagation channel compound system at both the Tx and Rx sides characterized by its covariance matrix [24].

3.2 Propagation Scenarios

For the sake of completeness, we consider a full set of propagation scenarios classified as 3-D uniform, 3-D omnidirectional, and 3-D directional. Considering the dual polarization case as in [53], 3-D propagation scenarios can be

characterized by the PAS of vertically and horizontally polarized incident waves $P_\vartheta(\Omega)$, $P_\phi(\Omega)$, respectively [54]. Ω denotes the solid angle of the 3-D space containing the incident waves under the mapping $\Omega \rightarrow \theta, \phi$ [55], where $\theta \in [0, \pi]$, $\phi \in [0, 2\pi]$ are the elevation and azimuth angles of incidence, respectively.

For 3-D uniform scenarios, i.e., 3-D isotropic, we have [56]

$$P_\vartheta(\Omega) = P_\vartheta(\theta, \phi) = P_\phi(\Omega) = P_\phi(\theta, \phi) = 1/(4\pi) \quad (1)$$

For 3-D directional scenarios, the Gaussian PAS is considered as [57]

$$P_\vartheta(\Omega) = P_\vartheta(\theta, \phi) = A_\vartheta \exp\left[-\frac{\{\theta - [(\pi/2) - m_V]\}^2}{2\sigma_V^2}\right] \exp\left[-\frac{(\phi - A_V)^2}{2S_V^2}\right] \quad (2)$$

$$P_\phi(\Omega) = P_\phi(\theta, \phi) = A_\phi \exp\left[-\frac{\{\theta - [(\pi/2) - m_H]\}^2}{2\sigma_H^2}\right] \exp\left[-\frac{(\phi - A_H)^2}{2S_H^2}\right] \quad (3)$$

where m_V and m_H are the mean elevation angles of the vertically and horizontally polarized waves, with standard deviations σ_V and σ_H , respectively. A_V and A_H are the mean azimuth angles of the vertically and horizontally polarized waves, with standard deviations S_V and S_H , respectively. For 3-D omnidirectional scenarios, the PAS is defined as [53]

$$P_\vartheta(\Omega) = P_\vartheta(\theta, \phi) = A_\vartheta \exp\left[-\frac{\{\theta - [(\pi/2) - m_V]\}^2}{2\sigma_V^2}\right] \quad (4)$$

$$P_\phi(\Omega) = P_\phi(\theta, \phi) = A_\phi \exp\left[-\frac{\{\theta - [(\pi/2) - m_H]\}^2}{2\sigma_H^2}\right] \quad (5)$$

The parameters A_ϑ and A_ϕ are constant values arising from the following relationship [57]

$$\int_\Omega P_\vartheta(\Omega) d\Omega = \int_0^{2\pi} \int_0^\pi P_\vartheta(\theta, \phi) \sin\theta d\theta d\phi = \int_\Omega P_\phi(\Omega) d\Omega = \int_0^{2\pi} \int_0^\pi P_\phi(\theta, \phi) \sin\theta d\theta d\phi = 1 \quad (6)$$

4 Key Performance Metrics

This Section derives the KPMs characterizing the performance of MPAs. The starting point is the covariance matrix formula characterizing the correlation between the port voltages. The DAG, CC, and EE are presented after that.

4.1 Covariance Matrix

The covariance matrix Λ of an N -port antenna is an $N \times N$ square matrix, with its i, j element defined as [25], [58]

$$\Lambda_{i,j} = \sqrt{(\rho_{env})_{i,j} \Gamma_i \Gamma_j} \quad (7)$$

where, Γ_i and Γ_j are the mean signal to noise ratio (SNR) at the i -th and j -th port respectively; and $(\rho_{env})_{i,j}$ is the ECC between the i -th and j -th port. The mean SNR of each antenna port is related to MEG of that port by applying [26]

$$\Gamma_n = \Gamma_0 G_{en} \quad (8)$$

where n is the number assigned to each port, Γ_0 is the reference mean SNR, and G_{en} is the MEG of n -th port. After substituting (8) in (7), we have

$$\Lambda_{i,j} = \Gamma_0 \sqrt{(\rho_{env})_{i,j} G_{ei} G_{ej}} \quad (9)$$

In the conventional covariance matrix formulation normalized to the reference SNR ($\Gamma_0=1$), the diagonal elements are equal to MEG of each port as seen in (9). The MEG is defined as [53]

$$G_{en} = \int_\Omega \left[\frac{\text{XPR}}{1+\text{XPR}} G_{\vartheta n}(\Omega) P_\vartheta(\Omega) + \frac{1}{1+\text{XPR}} G_{\phi n}(\Omega) P_\phi(\Omega) \right] d\Omega = \int_0^{2\pi} \int_0^\pi \left[\frac{\text{XPR}}{1+\text{XPR}} G_{\vartheta n}(\theta, \phi) P_\vartheta(\theta, \phi) + \right.$$

$$\frac{1}{1+\text{XPR}} G_{\varphi n}(\theta, \phi) P_{\varphi}(\theta, \phi) \sin\theta d\theta d\phi \quad (10)$$

where, XPR is the cross-polarization power ratio, $G_{\vartheta n}(\Omega)$ and $G_{\varphi n}(\Omega)$ are the ϑ and φ components of the antenna power gain pattern, respectively [53].

In the standardized dual-polarized, 3-D uniform propagation scenario, i.e., $\text{XPR}=1$, $P_{\vartheta}(\Omega) = P_{\varphi}(\Omega) = 1/(4\pi)$, the MEG of each port is always equal to 0.5 [53]. Thus, in such propagation scenario with uncorrelated port signals, i.e., $(\rho_{env})_{i,j} = 0$, $i \neq j$, the ideal format of the normalized covariance matrix ($\Gamma_0=1$) arises from (9) as:

$$\mathbf{\Lambda}_{\text{ideal}} = \begin{bmatrix} 0.5 & \cdots & 0 \\ \vdots & \ddots & \vdots \\ 0 & \cdots & 0.5 \end{bmatrix}_{N \times N} \quad (11)$$

Conventionally, DAG performance has been undertaken in 3-D uniform propagation scenarios [24], [27]. Thus, an optimum compound MPA system operating in a 3-D uniform propagation scenario will be one with covariance matrix as close as possible to (11). In directional propagation scenarios (non-uniform), the covariance matrix will have a different structure and the optimum MPA is subject to the antenna gain and orientation of the radiation pattern. The latter will be demonstrated in Section 5.

The covariance matrix formulation introduced in (9) does not rigorously and explicitly incorporate the radiation attributes and impedance matching of the MPA via standardized IEEE antenna terminology. The covariance matrix method that is adopted in this paper considers the radiation attributes and impedance matching of the MPA as independent factors [24]. It relies on the reciprocity principle and is calculated using the effective length matrix of the MPA without the need of determining the MEG and ECC. The equations for calculating the covariance matrix are [24]

$$\mathbf{\Lambda} = \Gamma_0 \frac{\omega \mu_0 k}{\pi Z_0} \mathbf{W} \left[\int_{\Omega} \mathbf{L}_e(\Omega) \mathbf{P}(\Omega) \mathbf{L}_e^H(\Omega) d\Omega \right] \mathbf{W}^H = \Gamma_0 \frac{\omega \mu_0 k}{\pi Z_0} \mathbf{W} \left[\int_0^{2\pi} \int_0^{\pi} \mathbf{L}_e(\theta, \phi) \mathbf{P}(\theta, \phi) \mathbf{L}_e^H(\theta, \phi) \sin\theta d\theta d\phi \right] \mathbf{W}^H \quad (12)$$

$$\mathbf{W} = (\mathbf{I} + \mathbf{Z}^T \mathbf{Z}_L^{-1})^{-1} \quad (13)$$

$$\mathbf{P}(\Omega) = \begin{bmatrix} \frac{\text{XPR}}{\text{XPR}+1} P_{\vartheta}(\Omega) & 0 \\ 0 & \frac{1}{\text{XPR}+1} P_{\varphi}(\Omega) \end{bmatrix} \quad (14)$$

where ω is the angular frequency, μ_0 is the free space permeability, k is the wavenumber, and Z_0 is the input impedance of the reference antenna which is 50Ω usually. \mathbf{Z} is the MPA impedance matrix and \mathbf{Z}_L is the impedance matrix of the MPA termination circuit. The superscripts H and T denote the matrix conjugate transpose and transpose, respectively. A typical 50Ω port termination is assumed in this paper. Thus, \mathbf{Z}_L is a 50Ω diagonal matrix [24]. $\mathbf{L}_e(\Omega)$ is the effective length matrix, incorporating the MPA radiation attributes defined as [27]

$$\mathbf{L}_e(\Omega) = \begin{bmatrix} \lambda_{\vartheta_1}(\Omega) & \lambda_{\varphi_1}(\Omega) \\ \lambda_{\vartheta_2}(\Omega) & \lambda_{\varphi_2}(\Omega) \\ \vdots & \vdots \\ \lambda_{\vartheta_N}(\Omega) & \lambda_{\varphi_N}(\Omega) \end{bmatrix} \quad (15)$$

where each row contains the ϑ and φ components of the effective length of each port. These components can be related to the antenna field pattern by applying [59]

$$\lambda_{\vartheta/\varphi}(\Omega) = j \frac{4\pi}{k\zeta I_{in}} E_{\vartheta/\varphi}(\Omega) = j \frac{2\lambda}{\zeta I_{in}} E_{\vartheta/\varphi}(\Omega) \quad (16)$$

where λ is the wavelength, ζ is the characteristic impedance of the propagation environment, and I_{in} is the input current to the antenna terminals. The effective length of each port is calculated by connecting a current source to the port and leaving the other ports unconnected [24], [27]. $E_{\vartheta/\varphi}(\Omega)$ accounts for the ϑ and φ components of the antenna radiation field pattern that can be extracted by the simulation software tool. $\mathbf{P}(\Omega)$ in eq. (14) accounts for the dual-polarized spatial propagation channel detailed in Section 3.2.

4.2 Diversity Antenna Gain

DAG characterizes the benefit achieved by applying the diversity principle [15]. The maximum theoretical DAG can be used to determine how optimum an MPA is. The DAG depends on the fading channel model and diversity combining technique. We consider the standardized Rayleigh, dual-polarized, 3-D uniform propagation scenario to analyze DAG. For an N-port antenna, the cumulative distribution function (CDF) of the output SNR in MRC diversity is defined as [24]

$$P(\gamma_{div} \leq x) = \int_0^x \sum_{i=1}^N \prod_{j=1, j \neq i}^N \left[\frac{\lambda_i}{\lambda_i - \lambda_j} \right] \frac{e^{-s/\lambda_i}}{\lambda_i} ds \quad (17)$$

where λ_i are the eigenvalues of the covariance matrix. For independent and identically distributed (IID) branches and MRC diversity, the CDF of SNR is given by [60]

$$P(\gamma_{div} \leq x) = 1 - e^{-x/\Gamma} \sum_{k=1}^N \frac{(x/\Gamma)^{k-1}}{(k-1)!} \quad (18)$$

where Γ is the mean received SNR. The DAG is calculated at 1% OP and is defined as [15]

$$DAG = \gamma_{div} / \gamma_{ideal} \quad (19)$$

where γ_{div} is the instantaneous SNR after diversity combining and γ_{ideal} is the instantaneous SNR of the ideal isotropic reference antenna that captures all incident power with CDF [24]

$$P(\gamma_{ideal} < x) = 1 - \exp(-x/\Gamma_0) \quad (20)$$

4.3 Channel Capacity

The ergodic CC in bits per second per Hertz (b/s/Hz) of a single-user MIMO channel is defined as [61]

$$C = E \left\{ \log_2 \left[\det \left(\mathbf{I} + \frac{P}{N_t \sigma_n^2} \mathbf{H}^H \mathbf{H} \right) \right] \right\} \quad (21)$$

where $E\{\cdot\}$ denotes the expectation operator, \mathbf{I} is the identity matrix with dimensions equal to the maximum number of antennas in Tx and Rx, P is the transmitted power, N_t is the number of Tx antenna elements, and σ_n^2 is the noise variance. The channel matrix \mathbf{H} has dimensions $N_r \times N_t$, where N_r is the number of Rx antenna elements. The general formula for calculating \mathbf{H} considering Rayleigh and Rician fading channels is [62]

$$\mathbf{H} = \sqrt{\frac{K}{K+1}} \mathbf{A} + \frac{1}{\sqrt{K+1}} \mathbf{V} \quad (22)$$

where, \mathbf{A} is a deterministic matrix which satisfies $(1/N_t) \times \text{Tr}(\mathbf{A} \mathbf{A}^H) = 1$. The constant $K \geq 0$ is the Rician K -factor. The matrix \mathbf{H} expresses a Rayleigh fading channel when $K = 0$. In a Kronecker correlation model, the matrix \mathbf{V} is determined by [62]

$$\mathbf{V} = \frac{1}{\sqrt{N_t}} \mathbf{\Lambda}_r^{1/2} \mathbf{U} \mathbf{\Lambda}_t^{1/2} \quad (23)$$

where \mathbf{U} is an $N_r \times N_t$ matrix with IID complex Gaussian random entries having zero mean and unit variance; $\mathbf{\Lambda}_r$ and $\mathbf{\Lambda}_t$ are the covariance matrices at the Rx and Tx MPA, respectively, derived by using eq. (12).

4.4 Energy Efficiency

The EE is defined as the number of information bits transmitted per Joule of energy [18], [19]

$$EE = BC / P_{tot} \quad (24)$$

where C is the ergodic CC, B is the bandwidth and P_{tot} is the total consumed power, defined as

$$P_{tot} = P + P_c \quad (25)$$

The circuit power P_c can be modelled as static [19]–[22] and dynamic [18], [23]. Considering P_c in (25) to be a fixed constant taking into account the power dissipated in the analog and digital circuitry of transceivers, P_{tot} is defined as

$$P_{tot} = P + P_s \quad (26)$$

where P_s denotes the static/fixed consumed circuit power. However, P_c is not fixed in practice but depends on bandwidth and CC. More realistic models were introduced in [18], [23] considering P_c to be dependent on the bandwidth and CC, thus P_{tot} can be expressed as

$$P_{tot} = P + P_d \quad (27)$$

where P_d denotes the dynamically consumed circuit power varying with bandwidth and CC. For comparison, in eq. (26), we consider the static circuit power model presented in [19], and in eq. (27), the dynamic circuit power model presented in [18] having

$$P_{tot} = P + P_d = P + \nu BN_t + \eta BN_t C \quad (28)$$

where νBN_t represents the power consumed by analog-to-digital and digital-to-analog converters, ν is a constant proportional to the sampling rate, $\eta BN_t C$ represents the power consumed by the encoder/decoder system, and η is a constant characterizing hardware.

5 MPA Performance Analysis

A comprehensive MPA performance analysis in 3-D uniform, omnidirectional, and directional propagation scenarios is presented in this Section. Both Rayleigh and Rician fading are considered. Such analysis will reveal the significance of EE as a complementary to DAG and CC KPMs in characterizing and classifying MPA systems. The strengths and limitations of each MPA in different propagation scenarios are also revealed guiding researchers towards devising or selecting optimum MPAs. The dual-port MPAs ($N=2$) [39], [31], [36], [52] are considered as case studies.

5.1 3-D Uniform Propagation Scenario

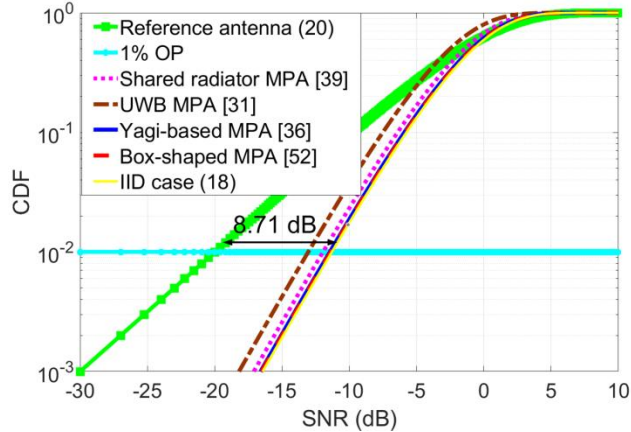
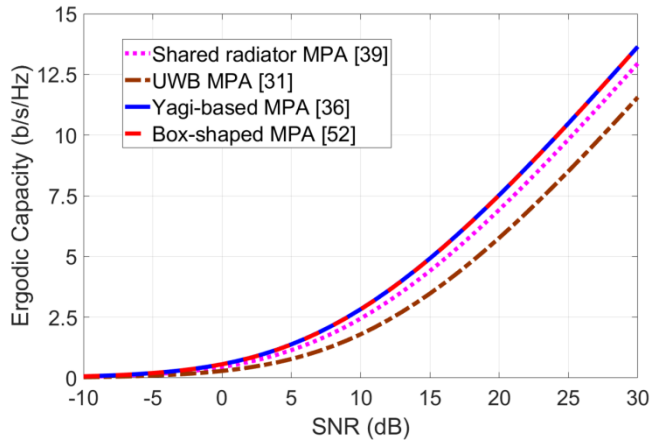
We begin with the simplest scenario which is the Rayleigh 3-D uniform propagation. It characterizes non-line-of-sight (NLOS) propagation which is usually the case in urban areas [7], [63]. Rayleigh dual-polarized, 3-D uniform propagation is the standardized scenario when studying diversity performance, comparing MPAs according to their exclusive radiation pattern attributes [6], [24], [27]. The covariance matrix is calculated first, followed by DAG, CC, and EE calculations for each MPA system.

The box-shaped MPA and the three selected MPAs reviewed in Section 2 are simulated using the CST tool. Their radiation pattern and impedance matching data are exported and applied into the covariance matrix equation in (12). The matrix $\mathbf{P}(\Omega)$ (eq. (14)) is determined considering the standardized dual-polarized ($XPR=1$), 3-D uniform propagation scenario presented in Section 3.2 (eq. (1)). The calculated covariance matrices are shown in Table 1. The diagonal elements of the covariance matrix can take any value from 0 to 0.5 in the dual-polarized, 3-D uniform scenario depending on the MPA radiation attributes and impedance matching. The non-diagonal elements of the matrix represent the correlation between the ports. It can be inferred from Table 1 that the box-shaped MPA offers the best performance compared with other works because its covariance matrix is closer to the ideal format derived in (11). The covariance matrix of the Yagi-based MPA is also close to the ideal format. By studying the covariance matrices and comparing them with the ideal covariance matrix, we can get an idea about the performance of MPAs even before determining the KPMs. Hence, we anticipate the box-shaped and Yagi-based MPAs to have higher DAG, CC, and EE compared to the others.

The next step is to determine the DAG using the CDFs of the output SNR in MRC diversity as explained in Section 4.2. The eigenvalues of each covariance matrix are calculated and employed in (17) ($N=2$). The CDFs of all four designs are depicted in Fig. 2. The CDF for the dual-branch IID case and that of the isotropic reference antenna in Rayleigh fading are also plotted applying (18) ($N=2$) and (20), respectively, with $\Gamma=\Gamma_0=1$. It is shown in Fig. 2 that the box-shaped MPA offers the highest DAG at 1% OP level which is equal to 8.63 dB. This value is very close to the maximum

Table 1. Covariance matrix: 3-D uniform propagation scenario.

MPA	Shared radiator [39]	UWB [31]	Yagi-based [36]	Box-shaped [52]
Covariance matrix	$\begin{bmatrix} 0.43 & 0.01 \\ 0.01 & 0.43 \end{bmatrix}$	$\begin{bmatrix} 0.33 & 0.02 \\ 0.02 & 0.33 \end{bmatrix}$	$\begin{bmatrix} 0.48 & -0.001 \\ -0.001 & 0.48 \end{bmatrix}$	$\begin{bmatrix} 0.49 & 0.006 \\ 0.006 & 0.49 \end{bmatrix}$

**Fig. 2.** CDF of SNR in the 3-D uniform propagation scenario.**Fig. 3.** Ergodic CC in the 3-D uniform propagation scenario.

theoretical limit of 8.71 dB achieved by the dual MRC with IID branches as can be seen in Fig. 2. The Yagi-based MPA achieves the second highest DAG, i.e., 8.57 dB, as expected by the covariance matrices in Table 1.

In the next step, the CC in Rayleigh fading is calculated as described in Section 4.3. The K factor in (22) is set equal to 0 for having a Rayleigh fading channel matrix. The noise variance in (21) is set equal to 1. Monte Carlo algorithm with 2500 iterations is used to calculate the CC of each MPA applying (21). The CCs of all four designs against SNR are depicted in Fig. 3. Although the CCs are close to each other, it is clear the box-shaped and Yagi-based MPAs offer the highest CC.

The EE in Rayleigh fading is then calculated using both the simplified static and more realistic dynamic power consumption models introduced in (26) and (28), respectively. In order to find EE using (26), P_c should be determined first. We employ (28) to heuristically determine P_c considering a fixed value for CC, i.e., $C = C_{med}$. Thus

$$P_c = \nu BN_t + \eta BN_t C_{med} \quad (29)$$

where C_{med} is the median capacity of the system. To determine the values of B and C_{med} , we should refer to the IEEE 802.11p standard for V2V communications [64]. The frequency range of this standard comprises of seven channels, where each channel has a bandwidth of 10 MHz. Thus, $B=10$ MHz is assumed in all calculations. According to the standard, the data rate per channel is in the range of 3-27 Mb/s which can assign a median value of 15 Mb/s. Thus, we set the C_{med} to the fixed value of 15 Mb/s. The values: $\nu = 10^{-14}$ J and $\eta = 10^{-15}$ J/bit are assumed in (29) based on the fundamental bound of computing power [18]. The EE of the four designs with respect to the transmit power using the

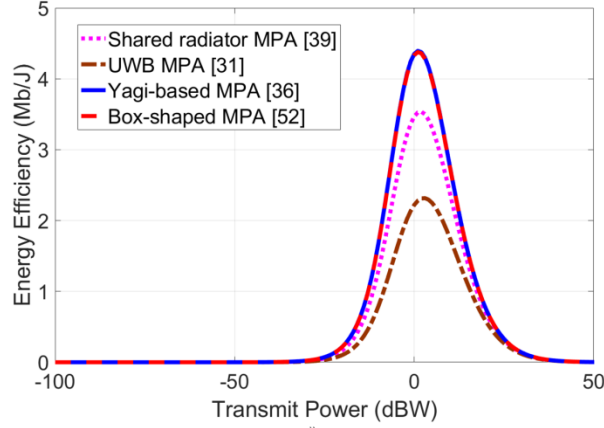


Fig. 4. EE in the 3-D uniform propagation scenario using the static circuit power consumption model (26) [19].

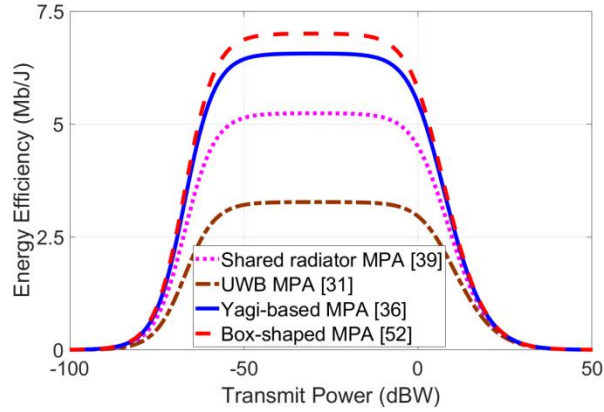


Fig. 5. EE in the 3-D uniform propagation scenario using the dynamic circuit power consumption model (28) [18].

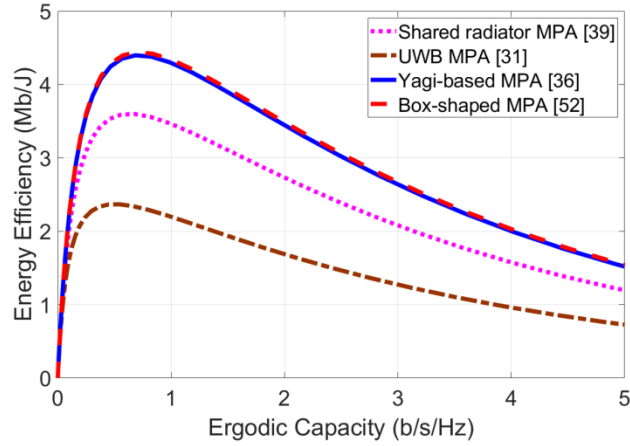
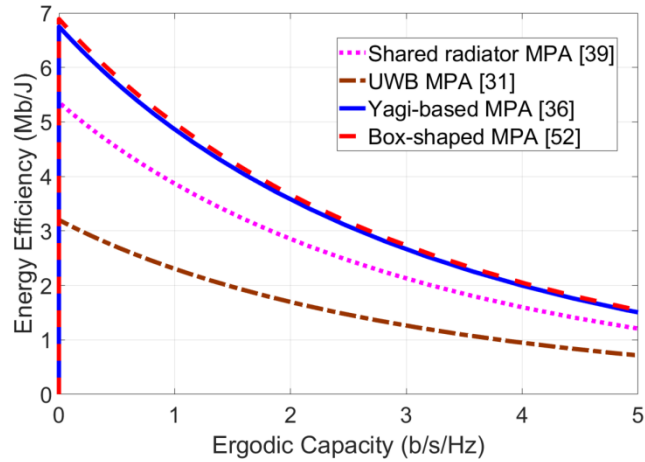
simplified static power consumption model (eq. (26)) [19] is shown in Fig. 4. Next, we employ the dynamic circuit power model (eq. (28)) [18]. The consumed power in the circuitry is related to the capacity which is not fixed but varies according to the transmit power. Again, we assume the values: $B = 10$ MHz, $\nu = 10^{-14}$ J, and $\eta = 10^{-15}$ J/bit in (28). The EE of the four designs with respect to the transmit power using the realistic dynamic power consumption model is depicted in Fig. 5. Figs. 4 and 5 confirm the box-shaped MPA is the most energy efficient design in this scenario. This was already expected as its covariance matrix is closer to the ideal format leading to higher DAG and CC compared with the other MPAs.

An important finding is that the box-shaped and Yagi-based MPAs cannot be sufficiently discriminated via the DAG and CC as shown in Figs. 2 and 3, respectively. This was made possible via the EE KPM when adopting the dynamic circuit power consumption model as shown in Fig. 5. That model will be adopted for the rest of the analysis. Moreover, the EE model with static circuit power [19] results in a single value of transmit power for EE maximization, whereas the EE model with dynamic circuit power [18] results in a range of transmit powers. The relationship between EE and CC has also been considered in the published literature [19]. However, this is not the proper way of presenting EE because CC also depends on transmit power. It is more intuitive to demonstrate EE with respect to transmit power as we did in Figs. 4 and 5 and was illustrated in [18] as well. We will follow this practice for the rest of this paper. However, to complete the performance analysis, we present EE versus CC for both static and dynamic circuit power models. The results are depicted in Figs. 6 and 7, respectively. The results of Fig. 6 show a similar trend to those presented in [19]. However, a more reasonable behavior of EE is revealed in Fig. 7 as EE monotonically decreases with increased CC. This is one more reason to adopt the dynamic circuit power consumption model of [18]. A comparison between the DAG, CC, and EE outcomes leads to two important findings:

- First, the CC and EE agree with DAG performance. In other words, the design with the highest DAG would offer the highest CC and EE. However, DAG and CC are in full compliance, a result that can be implicitly deduced from [16], [17]. Our analysis clearly confirmed that finding. We will focus on CC and EE for the rest of the analysis.
- Second, the performance of MPAs in 3-D uniform propagation does not depend on the gain and orientation of the radiation pattern but on the impedance matching, radiation efficiency and correlation between ports. Thus, well-designed MPAs with reasonable isolation and impedance matching would perform well in this scenario something

Table 2. Covariance matrix: 3-D omnidirectional propagation scenario.

MPA	Shared radiator [39]	UWB [31]	Yagi-based [36]	Box-shaped [52]
Covariance matrix	$\begin{bmatrix} 0.43 & 0.02 \\ 0.02 & 0.43 \end{bmatrix}$	$\begin{bmatrix} 0.36 & 0.11 \\ 0.11 & 0.36 \end{bmatrix}$	$\begin{bmatrix} 0.62 & -0.13 \\ -0.13 & 0.62 \end{bmatrix}$	$\begin{bmatrix} 0.52 & 0.004 \\ 0.004 & 0.69 \end{bmatrix}$

**Fig. 6.** EE versus ergodic CC in the 3-D uniform propagation scenario using the static circuit power consumption model (26) [19].**Fig. 7.** EE versus ergodic CC in the 3-D uniform propagation scenario using the dynamic circuit power consumption model (28) [18].

that was demonstrated in [37] for the Yagi-based MPA.

5.2 3-D Omnidirectional Propagation Scenario

A commonly used non-uniform propagation scenario is the omnidirectional one having Gaussian PAS in elevation and uniform PAS in azimuth [53]. Such a scenario is suitable for representing the propagation in urban environments and can be realistic for mobile and vehicular communication studies [53]. The covariance matrices of all four MPAs are determined in this scenario and the CC and EE are calculated in Rayleigh and Rician fading channels.

The process for calculating the covariance matrix is almost the same as in the 3-D uniform propagation scenario. The only difference is in determining the matrix $\mathbf{P}(\Omega)$, where eqs. (4) and (5) are employed in this scenario. It is assumed the vertically and horizontally polarized wave distributions are identical, and the mean elevation angle is equal to 30° to reflect a realistic urban propagation environment ($XPR = 1$, $m_V = m_H = 30^\circ \approx 0.5$ rad) [53]. The standard deviation in elevation is set to 0.5 radian ($\sigma_V = \sigma_H = 0.5$ rad). A_θ and A_ϕ are determined applying (6) as $A_\theta = A_\phi = 0.16$.

The covariance matrices are shown in Table 2. It is observed that some of the diagonal elements are bigger than 0.5. In a non-uniform propagation scenario, the diagonal elements of the covariance matrix can exceed 0.5. The maximum achievable diagonal element in such scenario is equal to the maximum gain of the antenna as discussed in [53]. This requires the PAS to be centered within the direction of the maximum gain. However, this is unlikely to happen in real-

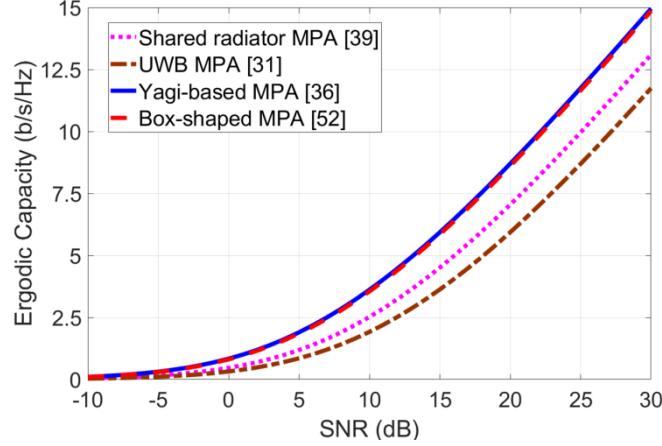


Fig. 8. Ergodic CC in the 3-D omnidirectional propagation scenario and Rayleigh fading.

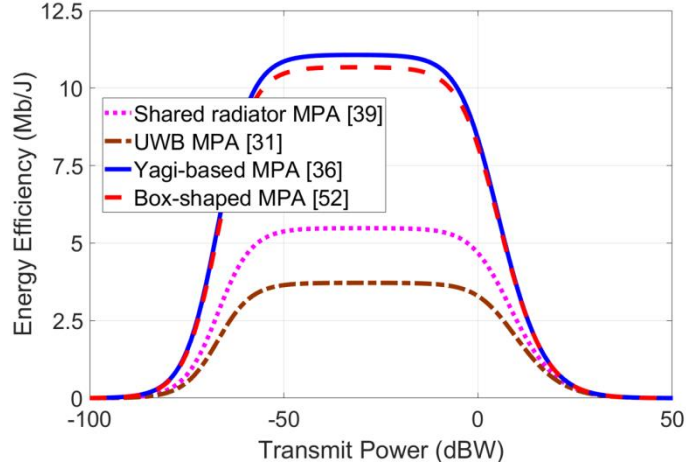


Fig. 9. EE in the 3-D omnidirectional propagation scenario and Rayleigh fading.

life scenarios. The CC and EE of all MPAs are calculated assuming Rayleigh fading and shown in Fig. 8 and Fig. 9, respectively. By comparing the results in Figs. 8 and 9 with the respective for 3-D uniform propagation in Figs. 3 and 5, it is understood the box-shaped and Yagi-based MPAs perform even better in 3-D omnidirectional propagation scenarios. The covariance matrix results of Table 2 can confirm that these two MPAs perform better because they have greater diagonal elements. Thus, both MPAs are suitable for urban propagation environments. Comparing the covariance matrices and CC and EE performances in such propagation scenario, the following important findings can be drawn:

- The radiation pattern orientation is also a determining factor in non-uniform propagation scenarios in addition to gain, radiation efficiency, and impedance matching of the MPA.
- The MPAs with radiation patterns evenly distributed in the azimuth plane perform better in this scenario. It can be either a low gain MPA with almost even pattern in azimuth or a high gain MPA with radiation pattern of elements evenly arranged in azimuth as in the box-shaped and Yagi-based MPAs.

Rician fading is considered next to account for the existence of a direct LOS path. The CC is calculated as described in Section 4.3. The K factor in (22) is set equal to 1. The CC and EE are depicted in Fig. 10 and Fig. 11, respectively. Although the CC and EE plots of the four MPAs are close to each other in this scenario, it is evident the box-shaped and Yagi-based MPAs perform better. An important finding in this scenario is:

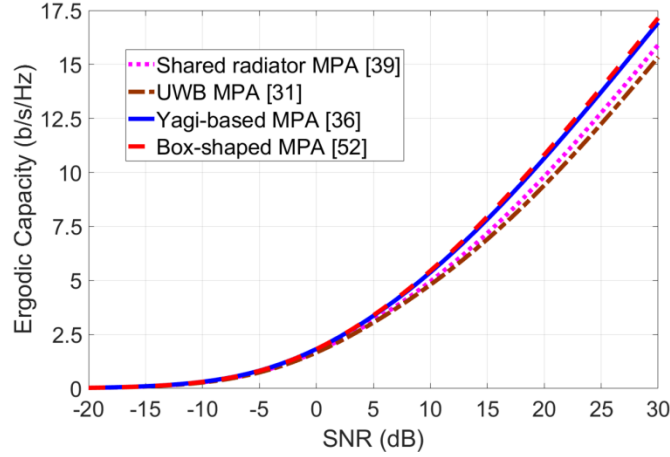
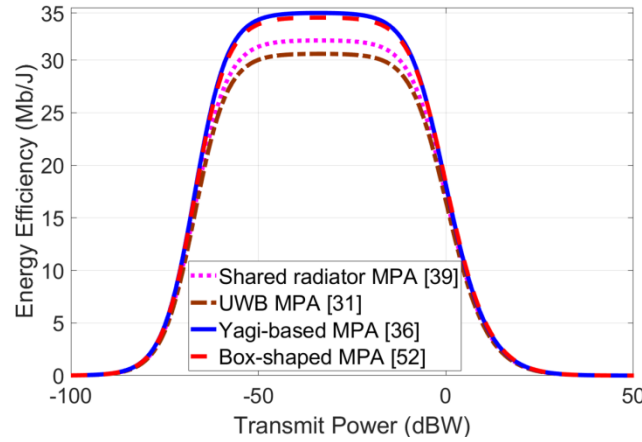
- In LOS propagation scenarios, CC and EE of different MPAs can get close to each other. The effect of the LOS component in Rician fading dominates performance behavior with the MPAs resembling a directional antenna. The design with higher gain performs better compared with others in this scenario. That is why the box-shaped and Yagi-based MPAs perform better.

5.3 3-D Directional Propagation Scenario

Another non-uniform propagation scenario is the 3-D directional having Gaussian PAS in both elevation and azimuth

Table 3. Covariance matrix: 3-D directional propagation scenario.

MPA	Shared radiator [39]	UWB [31]	Yagi-based [36]	Box-shaped [52]
Covariance matrix	$\begin{bmatrix} 1.09 & -0.4 + 0.5i \\ -0.4 + 0.5i & 0.97 \end{bmatrix}$	$\begin{bmatrix} 0.46 & 0.2 \\ 0.2 & 0.46 \end{bmatrix}$	$\begin{bmatrix} 1.29 & -0.29 \\ -0.29 & 1.29 \end{bmatrix}$	$\begin{bmatrix} 1.95 & 0.17 - 0.2i \\ 0.17 - 0.2i & 0.54 \end{bmatrix}$

**Fig. 10.** Ergodic CC in the 3-D omnidirectional propagation scenario and Rician fading.**Fig. 11.** EE in the 3-D omnidirectional propagation scenario and Rician fading.

[57]. This can be used to study MPA performance mainly in LOS scenarios. Such a scenario can be suitable for open environments but can also be adopted when designing MPAs for mm-wave wireless and vehicular communications. The covariance matrices are calculated first, and the CC and EE are determined for both Rayleigh and Rician fading.

To have a fair performance comparison in this scenario, the direction of maximum PAS should be exactly aligned with one of the main radiation pattern lobes of each MPA. The matrix $\mathbf{P}(\Omega)$ (eq. (14), XPR=1) is calculated using eqs. (2) and (3) with zero mean elevation and azimuth angle ($m_V = m_H = A_V = A_H = 0$). The standard deviation in both elevation and azimuth is set to 0.5 radian ($\sigma_V = \sigma_H = S_V = S_H = 0.5$). The constant values of A_ϑ and A_ϕ are determined by applying (6) as $A_\vartheta = A_\phi = 1.44$. The covariance matrices are shown in Table 3. It is observed that the diagonal elements of the covariance matrices have increased significantly due to the highly directional nature of this propagation scenario. Such an increase is not necessarily symmetric and depends on the radiation attributes of each MPA element. For example, the first diagonal element in the covariance matrix of the box-shaped MPA has increased to 1.95 according to Table 3 but the second diagonal element is only 0.54. This means the first element of the MPA that is aimed towards the arriving signal is receiving significantly more power than the other element which is aimed towards another direction. The non-diagonal elements have also increased significantly. It can be deduced:

- The correlation between the antenna ports is heavily influenced by the propagation scenario.
- The correlation between the antenna ports increases when the maximum gain direction of both elements is aimed

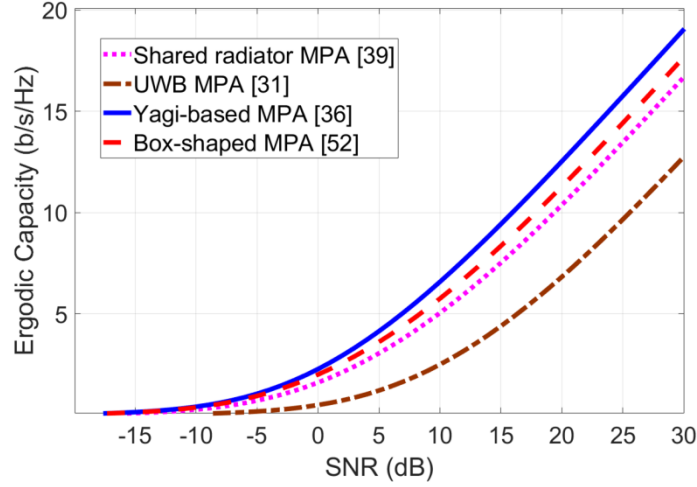


Fig. 12. Ergodic CC in the 3-D directional propagation scenario and Rayleigh fading.

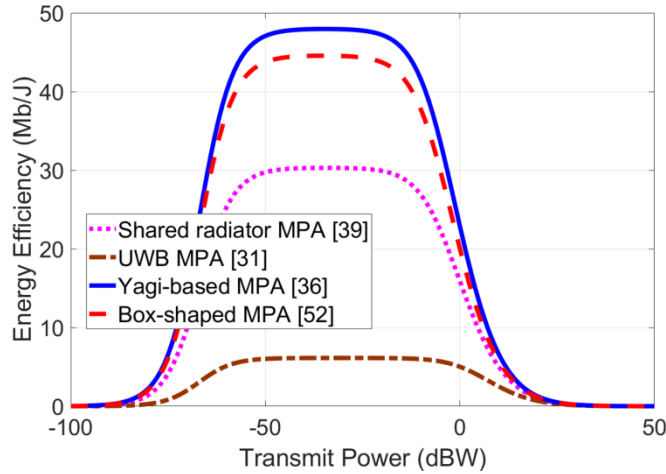


Fig. 13. EE in the 3-D directional propagation scenario and Rayleigh fading.

towards the direction of maximum PAS.

CC and EE are determined in Rayleigh fading using the covariance matrices of Table 3. The results are illustrated in Fig. 12 and Fig. 13, respectively. Since the diagonal elements of the covariance matrices are greater in this scenario compared to the previous ones, the maximum achievable CC and EE increases as shown Figs. 12 and 13. It is also shown that the Yagi-based MPA performs better than the other designs. The reason is that both antenna elements in the Yagi-based MPA are aimed almost towards the same direction. Therefore, both antennas receive the same amount of power which doubles the total amount of received power by the MPA. This fact can be confirmed by investigating the values of the covariance matrix elements in Table 3. The box-shaped MPA also shows good performance in this scenario despite having the radiation pattern of its antenna elements aimed towards different directions. The reason of such a good performance is its high gain which increases the first diagonal element in the covariance matrix to 1.95 as can be seen in Table 3. The second diagonal element is equal to 0.54 which means still a reasonable portion of power can be received by the back lobe of the other antenna element.

Finally, the similar analysis is done considering Rician fading. The Rician K factor in (22) is set equal to 1 in the calculations. CC and EE are depicted in Fig. 14 and Fig. 15, respectively. The performances show a similar trend with Rayleigh fading. However, performances are closer to each other as the LOS component dominates once it is fully received by the MPAs. A closer look on Figs. 14 and 15 leads to the finding:

- The shared radiator MPA is in the second position in terms of performance for SNR values more than 0 dB. It is evident from Table 3 that the elements of this design have the highest correlation. When the radiation patterns of the elements are aimed towards the same direction and the correlation between them is high, the MPA resembles a directional antenna and performs better in LOS Rician environments.

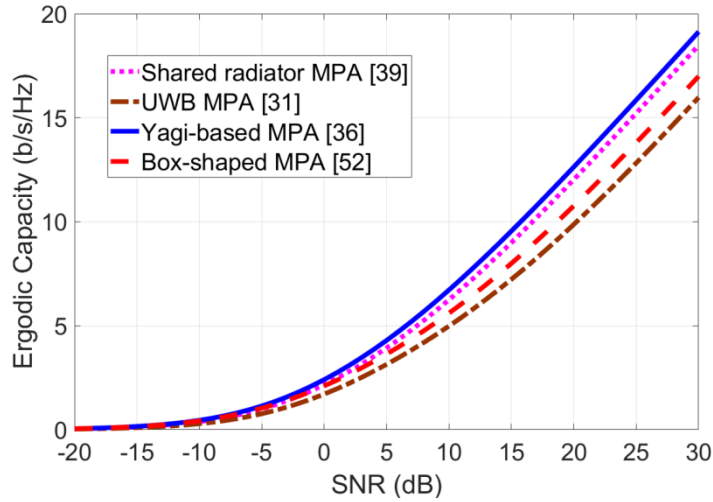


Fig. 14. Ergodic CC in the 3-D directional propagation scenario and Rician fading.

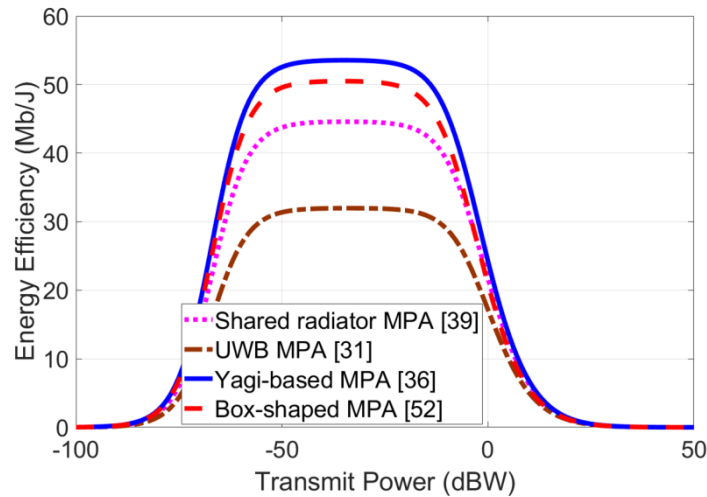


Fig. 15. EE in the 3-D directional propagation scenario and Rician fading.

5.4 Discussion

In summary, the analysis in Section 5.1 on the 3-D uniform propagation scenario showed the impedance matching and port isolation are two critical factors that influence MPA performance. In addition to these factors, it was revealed in Section 5.2 that the gain and radiation pattern of the antenna elements are also determining factors in 3-D omnidirectional propagation scenarios. In such scenarios, the radiation patterns of the antenna elements have to be evenly distributed around the azimuth to enhance performance. In the 3-D directional scenario in Section 5.3, the MPAs perform better when the maximum gain of both antenna elements is aimed towards the direction of maximum PAS. The analysis on Rician fading channels for both scenarios in Sections 5.2 and Section 5.3 concluded that pattern diversity cannot improve the performance in LOS scenarios, and it is better to have the maximum gain of both antenna elements towards the same direction. This would increase the correlation between the port voltages which has been found to be beneficiary in LOS scenarios. Overall, the box-shaped [52] and Yagi-based MPAs [36] have shown better performance in all propagation scenarios. These two MPAs not only offer high gain, good impedance matching, and high port isolation, but also have their radiation patterns well designed to accommodate directional propagation scenarios. Outstanding performance of the Yagi-based MPA in the 3-D uniform propagation scenario was also verified in [37] with the aid of the diversity measure metric leveraging MPA's covariance matrix. Such outstanding performance demonstrated here through the comprehensive use of DAG, CC, and EE is thus in alignment with the findings of [37]. As performance superiority of the Yagi-based MPA was confirmed in the remaining scenarios, i.e., 3-D omnidirectional and 3-D directional propagation in both Rayleigh and Rician fading, such finding complements [37] establishing the Yagi-based MPA [36] as an evidently superior design.

Table 4. Comparison between recent works in the literature.

Ref.	Size (mm ³)	Port distance (mm)	S11 at 5.9 GHz (dB)	S21 at 5.9 GHz (dB)	Gain at 5.9 GHz (dBi)	Propagation scenario	Fading channel	Performance metrics
[39]	39×39×0.8	34.6	-16	-15	4.5	3-D uniform	N/A	ECC
[31]	42×24×0.8	26	-10	-12	3.1	3-D uniform	Rayleigh	ECC, DAG
[36]	80×50×0.76	38.2	-25	-30	6	N/A	N/A	N/A
[29]	34×18×1.6	22.25	-10	-16	2.45	3-D uniform	Rayleigh	ECC, MEG, TARC, DAG
[30]	50×30×7.1	40.5	-15	-20	3	3-D uniform	Rayleigh	ECC, MEG, TARC, DAG
[28]	26×16×1.6	14	-10	-22	3.3	3-D uniform	Rayleigh	ECC, TARC, DAG
[40]	92×50×0.5	12	-15	-35	4	3-D uniform	Rayleigh	ECC, DAG
[34]	46×26×1.6	34.5	-4.9	-23	N/A	3-D uniform	Rayleigh	ECC, DAG, CC loss
[52]	36×36×25.8	26.4	-10.6	-21	6.5	3-D uniform	Rayleigh	DAG

The comparison between state-of-the-art MPAs is summarized in Table 4. This table contains the size details and specifications of the antenna elements such as S-parameters and gain. It is also depicted how evaluation in terms of propagation environment, fading channel model, and KPMs was conducted. As we can see, the box-shaped MPA [52] offers the highest gain of 6.5 dBi and port isolation of 21 dB despite the short distance between the antenna ports. The Yagi-based MPA [36] also offers a high gain and port isolation, but this is achieved at the expense of a larger size and port distance. The last three columns of Table 4 show that most of the previous works studied the performance in just the standardized Rayleigh 3-D uniform propagation scenario. Here we analyzed performance of state-of-the-art MPAs in 3-D uniform, 3-D directional, and 3-D omnidirectional propagation scenarios considering both Rayleigh and Rician fading. The ECC seems to be one of the most popular metrics in literature. However, we did not need to calculate this metric as we employed a state-of-the-art electromagnetic-based covariance matrix methodology that quantifies the impact of the different components constituting the whole MPA system, i.e., a) termination circuit, b) MPA, c) wireless propagation channel (see also Fig. 1).

According to the details given in Table 4 and the performance analysis conducted previously, the box-shaped [52] and Yagi-based MPAs [36] show optimum performance features compared with other state-of-the-art MPAs. In fact, the more uniform the propagation scenario becomes, the higher the performance superiority of the box-shaped MPA is. On the contrary, the more directional the propagation scenario becomes the higher the performance superiority of the Yagi-based MPA is. The UWB MPA [31] looks like the smallest and simplest one to design, but its performance is always inferior. Only, in LOS Rician omnidirectional propagation scenarios, it can come relatively closer to others. Such remarks can constitute important guidelines for wireless systems designers/engineers towards selecting an MPA that suits their needs. Research can be guided towards incorporating performance evaluation aspects as in this paper before releasing an MPA design. The presented analysis can be readily extended and benefit current and future state-of-the-art MPA research and technology such as 4-port optically transparent [12], [65], 4-port planar slot-based [66], and 4-port vehicle-mounted [67].

6 Conclusion

A comprehensive and complete performance analysis of MPA systems was presented. Results on dual-port antennas operating in the 5.9 GHz band for V2V communications were considered as case study. DAG, CC, and EE were employed as a complete set of KPMs to analyze performance. EE can sufficiently characterize performance and compare MPAs when DAG and CC fail to do so. Given peoples' emerging environmental concerns, the importance of employing EE to characterize wireless systems performance is well understood. The analysis considered all classes of wireless propagation scenarios, namely, 3-D uniform, 3-D directional, and 3-D omnidirectional scenarios, in both Rayleigh and Rician fading. We derived the ideal form of the covariance matrix in the standardized dual-polarized, 3-D uniform propagation scenario as a means of informing optimum MPA design and calibration. MPAs that approach such covariance matrix form are anticipated to approach optimum performance. We analyzed a proof-of-concept box-shaped MPA with covariance matrix similar to the ideal one in the standardized dual-polarized, 3-D uniform propagation scenario. After comparisons with published state-of-the-art designs, the proof-of-concept MPA showed optimum performance features across all wireless propagation scenarios. The presented performance analysis methodology can be readily extended to designs with more ports and in different frequency bands and communication channels. It can facilitate the selection of MPAs meeting certain performance and size requirements and open new pathways in MPA

design underpinned by optimum performance. Research can be guided in such direction before releasing an MPA.

7 Declarations

7.1 Funding

This work was supported by the Engineering and Physical Sciences Research Council (EPSRC) under grant EP/R027641/1: Bandwidth and Energy Efficient Compact Multi-Antenna Systems for Connected Autonomous Vehicles.

7.2 Competing Interests

The authors have no relevant financial or non-financial interests to disclose.

7.3 Availability of Data and Material

Data sharing not applicable to this article as no datasets were generated or analyzed during the current study.

7.4 Code Availability

Code availability not applicable to this article as no codes were generated or analyzed during the current study.

7.5 Authors' Contributions

All authors contributed to the study conception and design. All authors commented on previous versions of the manuscript. All authors read and approved the final manuscript.

8 References

1. WWRF, "Wireless Communication Using Higher Frequency Bands," White Paper 5, no. 23, 2017. [online] available at <https://www.wwrf.ch/files/content%20wwrf/publications/outlook/Outlook23.pdf>.
2. M. Fallgren et al., "Fifth-Generation Technologies for the Connected Car: Capable Systems for Vehicle-to-Anything Communications," *IEEE Veh. Technol. Mag.*, vol. 13, no. 3, pp. 28-38, 2018.
3. B. I. Yaqoob et al., "Internet of Things Architecture: Recent Advances, Taxonomy, Requirements, and Open Challenges," *IEEE Wireless Commun.*, vol. 24, no. 3, pp. 10-16, 2017.
4. G. D. Durgin, "Space-time wireless channels," Prentice Hall, 2003.
5. S. K. Yong and J. S. Thompson, "Three-dimensional spatial fading correlation models for compact MIMO receivers," *IEEE Trans. Wireless Commun.*, vol. 4, no. 6, pp. 2856-2869, 2005.
6. V. C. Papamichael and P. Karadimas, "Performance evaluation of actual multielement antenna systems under transmit antenna selection/maximal ratio combining," *IEEE Antennas Wireless Propag. Lett.*, vol. 10, pp. 690-692, 2011.
7. P. Karadimas and J. Zhang, "A generalized analysis of three-dimensional anisotropic scattering in mobile wireless channels-Part I: Theory," *2011 IEEE Veh. Technol. Conf. (VTC Spring)*, pp. 1-5, 2011.
8. S. Sangodoyin et al., "Cluster characterization of 3-D MIMO propagation channel in an urban macrocellular environment," *IEEE Trans. Wireless Commun.*, vol. 17, no. 8, pp. 5076-5091, 2018.
9. L. Zhang, Z. Luo, and S.-H. Leung, "An Efficient Approximation of Spatial Correlation Based on Gauss-Hermite Quadrature," *IEEE Trans. Signal Process.*, vol. 66, no. 3, pp. 617-626, 2017.
10. Forenza, D. J. Love, and R. W. Heath, "Simplified spatial correlation models for clustered MIMO channels with different array configurations," *IEEE Trans. Veh. Technol.*, vol. 56, no. 4, pp. 1924-1934, 2007.
11. Y. Huang, P. Karadimas and A. Pour Sohrab, "Spatial Channel Degrees of Freedom for Optimum Antenna Arrays," *IEEE Trans. Wireless Commun.*, vol. 22, no. 8, pp. 5129-5144, 2023.
12. Y. Yao, Y. Shao, J. Zhang and J. Zhang, "A Transparent Antenna Using Metal Mesh for UWB MIMO Applications," *IEEE Trans. Antennas Propag.*, vol. 71, no. 5, pp. 3836-3844, 2023.
13. O. Kaiwartya et al., "Internet of vehicles: Motivation, layered architecture, network model, challenges, and future aspects," *IEEE Access*, vol. 4, pp. 5356-5373, 2016.
14. M. S. Sharawi, "Printed multi-band MIMO antenna systems and their performance metrics," *IEEE Antennas Propag. Mag.*, vol. 55, no. 5, pp. 218-232, 2013.
15. P. S. Kildal, K. Rosengren, J. Byun, and J. Lee, "Definition of effective diversity gain and how to measure it in a reverberation chamber," *Microw. Opt. Technol. Lett.*, vol. 34, no. 1, pp. 56-59, 2002.
16. S. Loyka and A. Kouki, "New compound upper bound on MIMO channel capacity," *IEEE Commun. Lett.*, vol. 6, no. 3, pp. 96-98, 2002.

17. B.T. Quist and M. A. Jensen, "Optimal antenna radiation characteristics for diversity and MIMO systems," *IEEE Trans. Antennas Propag.*, vol. 57, no. 11, pp. 3474-3481, 2009.
18. E. Björnson and E. G. Larsson, "How energy-efficient can a wireless communication system become?," *2018 IEEE 52nd Asilomar Conf. Signals, Systems, and Computers*, pp. 1252-1256, 2018.
19. J. Jiang, M. Dianati, M. A. Imran, R. Tafazolli, and Y. Chen, "On the relation between energy efficiency and spectral efficiency of multiple-antenna systems," *IEEE Trans. Veh. Technol.*, vol. 62, no. 7, pp. 3463-3469, 2013.
20. L. Deng, Y. Rui, P. Cheng, J. Zhang, Q. T. Zhang, and M. Li, "A unified energy efficiency and spectral efficiency tradeoff metric in wireless networks," *IEEE Commun. Lett.*, vol. 17, no. 1, pp. 55-58, 2013.
21. D. Tsilimantou, J. M. Gorce, K. Jaffrès-Runser, and H. Vincent Poor, "Spectral and Energy Efficiency Trade-offs in Cellular Networks," *IEEE Trans. Wireless Commun.*, vol. 15, no. 1, pp. 54-66, 2016.
22. R. Zhang, Y. Li, C. X. Wang, Y. Ruan, Y. Fu, and H. Zhang, "Energy-Spectral Efficiency Trade-Off in Underlying Mobile D2D Communications: An Economic Efficiency Perspective," *IEEE Trans. Wireless Commun.*, vol. 17, no. 7, pp. 4288-4301, 2018.
23. J. Tang, D. K. C. So, E. Alsusa, K. A. Hamdi, and A. Shojaeifard, "On the Energy Efficiency-Spectral Efficiency Tradeoff in MIMO-OFDMA Broadcast Channels," *IEEE Trans. Veh. Technol.*, vol. 65, no. 7, pp. 5185-5199, 2016.
24. V. Papamichael and P. Karadimas, "On the Covariance Matrix and Diversity Performance Evaluation of Compact Multiport Antenna Systems," *IEEE Trans. Antennas Propag.*, vol. 65, no. 11, pp. 6140-6144, 2017.
25. M. Schwartz, W. R. Bennett, and S. Stein, "Communication systems and techniques," John Wiley & Sons, 1995.
26. J.-i. Takada and K. Ogawa, "Concept of diversity antenna gain," Paris, France, EURO-COST, vol. 273, 2003.
27. V. Papamichael and C. Soras, "Generalised Selection Combining Diversity Performance of Multi-Element Antenna Systems via a Stochastic Electromagnetic-Circuit Methodology," *IET Microw. Antennas Propag.*, vol. 4, no. 7, pp. 837-846, 2010.
28. T. Addepalli and V. R. Anitha, "Parametric Analysis of Compact UWB-MIMO Antenna with Improved Isolation Using Parasitic Reflectors and Protruded Ground Strips," *Wireless Pers. Commun.*, vol. 123, pp. 2209-2225, 2022.
29. R. Chandell, A. K. Gautam, and K. Rambabu, "Tapered Fed Compact UWB MIMO-Diversity Antenna with Dual Band-Notched Characteristics," *IEEE Trans. Antennas Propag.*, vol. 66, no. 4, pp. 1677-1684, 2018.
30. G. Das, A. Sharma, and R. K. Gangwar, "Wideband self-complementary hybrid ring dielectric resonator antenna for MIMO applications," *IET Microw. Antennas Propag.*, vol. 12, no. 1, pp. 108-114, 2017.
31. M. G. N. Alsath and M. Kanagasabai, "Compact UWB monopole antenna for automotive communications," *IEEE Trans. Antennas Propag.*, vol. 63, no. 9, pp. 4204-4208, 2015.
32. W. Li, Y. Hei, P. M. Grubb, X. Shi, and R. T. Chen, "Compact inkjet-printed flexible MIMO antenna for UWB applications," *IEEE Access*, vol. 6, pp. 50290-50298, 2018.
33. K. Gautam, S. Yadav, and K. Rambabu, "Design of ultra-compact UWB antenna with band-notched characteristics for MIMO applications," *IET Microw. Antennas Propag.*, vol. 12, no. 12, pp. 1895-1900, 2018.
34. Ibrahim, M. A. Abdalla, and Z. Hu, "Compact ACS-fed CRLH MIMO antenna for wireless applications," *IET Microw. Antennas Propag.*, vol. 12, no. 6, pp. 1021-1025, 2018.
35. S. Zhang and G. F. Pedersen, "Mutual coupling reduction for UWB MIMO antennas with a wideband neutralization line," *IEEE Antennas Wireless Propag. Lett.*, vol. 15, pp. 166-169, 2016.
36. S. S. Jehangir and M. S. Sharawi, "A miniaturized UWB biplanar Yagi-based MIMO antenna system," *IEEE Antennas Wireless Propag. Lett.*, vol. 16, pp. 2320-2323, 2017.
37. R. S. Kshetrimayum, M. Mishra, S. Aïssa, S. K. Koul and M. S. Sharawi, "Diversity Order and Measure of MIMO Antennas in Single-User, Multiuser, and Massive MIMO Wireless Communications," *IEEE Antennas Wireless Propag. Lett.*, vol. 22, no. 1, pp. 19-23, 2023.
38. J. Zhu, S. Li, B. Feng, L. Deng, and S. Yin, "Compact dual-polarized UWB quasi-self-complementary MIMO/diversity antenna with band-rejection capability," *IEEE Antennas Wireless Propag. Lett.*, vol. 15, pp. 905-908, 2015.
39. S. R. Patre and S. P. Singh, "Shared radiator MIMO antenna for broadband applications," *IET Microw. Antennas Propag.*, vol. 12, no. 7, pp. 1153-1159, 2018.
40. L. Y. Nie, X. Q. Lin, S. Xiang, B. Wang, L. Xiao and J. Y. Ye, "High-Isolation Two-Port UWB Antenna Based on Shared Structure," *IEEE Trans. Antennas Propag.*, vol. 68, no. 12, pp. 8186-8191, 2020.
41. R. Gómez-Villanueva and H. Jardón-Aguilar, "Compact UWB uniplanar four-port MIMO antenna array with rejecting band," *IEEE Antennas Wireless Propag. Lett.*, vol. 18, no. 12, pp. 2543-2547, 2019.
42. S. S. Jehangir and M. S. Sharawi, "A compact single-layer four-port orthogonally polarized Yagi-Like MIMO antenna system," *IEEE Trans. Antennas Propag.*, vol. 68, no. 8, pp. 6372-6377, 2020.
43. Y. S. Kim and D.-H. Cho, "Design of Four-Port Integrated Monopole Antenna Using Refraction Effect of Dielectric Medium for Pattern Gain Enhancement," *IEEE Antennas Wireless Propag. Lett.*, vol. 19, no. 4, pp. 621-625, 2020.
44. R. Anitha, P. Vinesh, K. Prakash, P. Mohanan, and K. Vasudevan, "A compact quad element slotted ground wideband antenna for MIMO applications," *IEEE Trans. Antennas Propag.*, vol. 64, no. 10, pp. 4550-4553, 2016.
45. A. Ramachandran, S. Mathew, V. Rajan, and V. Kesavath, "A compact triband quad-element MIMO antenna using SRR ring for high isolation," *IEEE Antennas Wireless Propag. Lett.*, vol. 16, pp. 1409-1412, 2016.
46. E. Fritz-Andrade, A. Perez-Miguel, R. Gomez-Villanueva, and H. Jardón-Aguilar, "Characteristic mode analysis applied to reduce the mutual coupling of a four-element patch MIMO antenna using a defected ground structure," *IET Microw. Antennas Propag.*, vol. 14, no. 2, pp. 215-226, 2019.
47. A. A. R. Saad and H. A. Mohamed, "Conceptual design of a compact four-element UWB MIMO slot antenna array," *IET*

- Microw. Antennas Propag.*, vol. 13, no. 2, pp. 208-215, 2019.
48. Mathur, Rohit, and Santanu Dwari, "8-port multibeam planar UWB-MIMO antenna with pattern and polarisation diversity," *IET Microw. Antennas Propag.*, vol. 13, no. 13, pp. 2297-2302, 2019.
 49. M. G. N. Alsath et al., "An Integrated Tri-Band/UWB Polarization Diversity Antenna for Vehicular Networks," *IEEE Trans. Veh. Technol.*, vol. 67, no. 7, pp. 5613-5620, July 2018.
 50. Das, Gourab, Nikesh Kumar Sahu, Anand Sharma, Ravi Kumar Gangwar, and Mohammad S. Sharawi. "Dielectric resonator-based four-element eight-port MIMO antenna with multi-directional pattern diversity." *IET Microw. Antennas Propag.*, vol. 13, no. 1, pp. 16-22, 2019.
 51. S. Koziel and A. Pietrenko-Dabrowska, "Rapid Variable-Resolution Parameter Tuning of Antenna Structures Using Frequency-Based Regularization and Sparse Sensitivity Updates," *IEEE Trans. Antennas Propag.*, vol. 70, no. 12, pp. 12177-12188, 2022.
 52. A. P. Sohrab, P. Karadimas and Y. Huang, "Covariance Matrix Evaluation of a Diversity Slot Antenna for Vehicular Communications," *2019 IEEE International Symposium on Antennas and Propagation and USNC-URSI Radio Science Meeting, Atlanta, GA, USA*, pp. 931-932, 2019.
 53. T. Taga, "Analysis for mean effective gain of mobile antennas in land mobile radio environments," *IEEE Trans. Veh. Technol.*, vol. 39, no. 2, pp. 117-131, 1990.
 54. K. Kalliola, K. Sulonen, H. Laitinen, O. Kivekäs, J. Krogerus, and P. Vainikainen, "Angular power distribution and mean effective gain of mobile antenna in different propagation environments," *IEEE Trans. Veh. Technol.*, vol. 51, no. 5, pp. 823-838, 2002.
 55. B. H. Fleury, "First- and second-order characterization of direction dispersion and space selectivity in the radio channel," *IEEE Trans. Inf. Theory*, vol. 46, no. 6, pp. 2027-2044, 2000.
 56. Y. F. Alem, Z. Khalid, and R. A. Kennedy, "3D spatial fading correlation for uniform angle of arrival distribution," *IEEE Commun. Lett.*, vol. 19, no. 6, pp. 1073-1076, 2015.
 57. Ando, T. Taga, A. Kondo, K. Kagoshima, and S. Kubota, "Mean effective gain of mobile antennas in line-of-sight street microcells with low base station antennas," *IEEE Trans. Antennas Propag.*, vol. 56, no. 11, pp. 3552-3565, 2008.
 58. V. C. Papamichael, "Selection-Combining Diversity Performance of Actual Multielement Antenna Systems Using the Covariance Matrix Method," *IEEE Antennas Wireless Propag. Lett.*, vol. 9, pp. 705-707, 2010.
 59. S. J. Orfanidis, "Electromagnetic waves and antennas," 2002. [online] available at <http://www.ece.rutgers.edu/~orfanidi/ewa>.
 60. A. Goldsmith, "Wireless communications," Cambridge Univ. Press, 2005.
 61. A. Goldsmith, S. A. Jafar, N. Jindal, and S. Vishwanath, "Capacity limits of MIMO channels," *IEEE J. Sel. Areas Commun.*, vol. 21, no. 5, pp. 684-702, 2003.
 62. J. Dumont, W. Hachem, S. Lasaulce, P. Loubaton, and J. Najim, "On the capacity achieving covariance matrix for Rician MIMO channels: an asymptotic approach," *IEEE Trans. Inf. Theory*, vol. 56, no. 3, pp. 1048-1069, 2010.
 63. P. Karadimas and D. Matolak, "Generic stochastic modeling of vehicle-to-vehicle wireless channels," *Veh. Commun.*, vol. 1, no. 4, pp. 153-167, 2014.
 64. E. C. Committee, "The European table of frequency allocations and applications in the frequency range 8.3 kHz to 3000 GHz (ECA table)," Proc. European Conf. Postal Telecommun. Administrations; Electronic Commun. Committee: Copenhagen, Denmark, 2013.
 65. L. Kannappan, et al., "Quad-port multiservice integrated optically transparent automotive antenna for vehicular classification applications," *Scientific reports*, 2023.
 66. A. D. Tadesse, O. P. Acharya, S. Sahu, "A wideband four-port multiple-input-multiple-output slot antenna for WLAN/WiFi/5G below 6 GHz applications," *Int. Journal RF Microw. Comput. Aided Eng.*, vol. 31, no. 5, 2021.
 67. J. -K. Che, C. -C. Chen and J. F. Locke, "A Compact Four-Channel MIMO 5G Sub-6 GHz/LTE/WLAN/V2X Antenna Design for Modern Vehicles," *IEEE Trans. Antennas Propag.*, vol. 69, no. 11, pp. 7290-7297, 2021.